Molecular Imaging
Volume 15: 1-8

DOI: 10.1177/1536012116646489
mix.sagepub.com
SAGE

Evaluation of a BGO-Based PET System for Single-Cell Tracking Performance by Simulation and Phantom Studies

Yu Ouyang, PhD[1], Tae Jin Kim, PhD[1], and Guillem Pratx, PhD[1]

Abstract

A recent method based on positron emission was reported for tracking moving point sources using the Inveon PET system. However, the effect of scanner background noise was not further explored. Here, we evaluate tracking with the Genisys4, a bismuth germanate-based PET system, which has no significant intrinsic background and may be better suited to tracking lower and/or faster activity sources. Position-dependent sensitivity of the Genisys4 was simulated in Geant4 Application for Tomographic Emission (GATE) using a static ^{18}F point source. Trajectories of helically moving point sources with varying activity and rotation speed were reconstructed from list-mode data as described previously. Simulations showed that the Inveon's ability to track sources within 2 mm of localization error is limited to objects with a velocity-to-activity ratio < 0.13 mm/decay, compared to < 0.29 mm/decay for the Genisys4. Tracking with the Genisys4 was then validated using a physical phantom of helically moving [^{18}F] fluorodeoxyglucose-in-oil droplets (< 0.24 mm diameter, 139-296 Bq), yielding < 1 mm localization error under the tested conditions, with good agreement between simulated sensitivity and measured activity (Pearson correlation $R = .64$, $P << .05$ in a representative example). We have investigated the tracking performance with the Genisys4, and results suggest the feasibility of tracking low activity, point source-like objects with this system.

Keywords

cell tracking, positron emission, single cell, GATE simulation, preclinical imaging

Introduction

Methods for spatiotemporal tracking cells are becoming increasingly important as interest in cell-based therapies continues to grow. Such methods can shed light on biodistribution and viability of cells, which may be important markers of treatment efficacy.[1] In addition, cell tracking is potentially valuable for studying circulating tumor cells, a key to understanding cancer metastasis.[2]

Current in vivo cell tracking methods are not ideal for following the trajectory of single cells throughout the whole body. For example, methods such as immunomagnetic capture[3] or optical imaging techniques[4] have been used with circulating tumor cells, but they are better suited for detection rather than tracking and are limited by tissue depth. Whole-body tracking of mesenchymal stem cells and circulating progenitor cells has been reported using positron emission tomography (PET),[5,6] but while cell tracking benefits from the sensitivity of PET, the tomography paradigm that represents data discretely in space and time is inappropriate for tracking of single or small numbers of cells.[7] While in vivo, whole-body detection of single cells has been demonstrated using magnetic resonance imaging (MRI),[8,9] single-cell tracking in a continuous manner using MRI has generally been limited to in vitro conditions.[10-12]

Tracking of single, positron-emitting particles was demonstrated as early as 1988[13] and later refined for industrial applications.[14] A similar but improved method for reconstructing the continuous spatiotemporal trajectory point-source–like objects was recently demonstrated in silico for the Inveon preclinical PET system (Siemens Healthcare Solutions USA, Knoxville, Tennessee) under the ideal case without background from the cerium-doped lutetium oxyorthosilicate (Lu_2SiO_5: Ce,

[1] Radiation Biophysics Laboratory, Department of Radiation Oncology, Stanford University, Palo Alto, CA, USA

Submitted: 02/10/2015. Revised: 05/02/2016. Accepted: 03/03/2016.

Corresponding Author:
Guillem Pratx, Stanford University, 1050 Arastradero Rd, A226, Palo Alto, CA 94304, USA.
Email: pratx@stanford.edu

Table 1. GATE Simulation Parameters.

Total simulated time, s	100
Length of time slice, ms	10
Range of activity, Bq	1-1000
Range of rotation speed, deg/s	4-1059
Rotation radius, mm	10
Axial translation speed, mm/s	0.4

Abbreviation: GATE, Geant4 Application for Tomographic Emission.

or LSO) scintillators.[7] However, intrinsic LSO background from ^{176}Lu is approximately equivalent to a 100 Bq source in the field of view (FOV),[15] which is unsuitable for tracking objects with low activities.

Here, we explore the feasibility of single-cell tracking using the Genisys4 (Sofie Biosciences, Culver City, California), a PET system with a more sensitive geometry and detectors based on bismuth germanate ($Bi_4Ge_3O_{12}$ or BGO),[16] which has insignificant intrinsic background.[17] We simulate the system in silico to characterize its sensitivity as well as its trajectory reconstruction performance compared to the Inveon system with and without LSO background. We then mimic cell tracking using a phantom consisting of moving, [^{18}F] fluorodeoxyglucose (FDG)-filled droplets and reconstruct their trajectory from list-mode data acquired with the Genisys4.

Materials and Methods

Monte Carlo Simulation in GATE

Both the Genisys4 and Inveon systems were simulated in Geant4 Application for Tomographic Emission (GATE 7.0). The source was a helically moving ^{18}F point source placed in a water cylinder (1.25 cm radius, 5 cm length), with parameters shown in Table 1 and described in the previous study.[7] Each Monte Carlo simulation was repeated 10 times with a different random seed for the purpose of statistical significance. For the Genisys4, an energy window of either 150 to 650 keV or 350 to 650 keV was used; the former is the default window on the system, whereas the latter is the value suggested in the literature to minimize backscatter.[18] The energy resolution was set to 18%, based on the mean full width at half maximum value measured in previous studies.[19] More details of the Genisys4 detector configuration are available in the literature.[20] Simulations of the Inveon without LSO background were based on configurations from previous studies[7] but with an optimal energy window of 350 to 650 keV for rejecting backscatter events.[15] For reconstruction purpose, the ends of the lines of response (LORs) were placed in the center of the frontal face of each crystal and at a fixed depth value as follows: 3.9 mm for LSO (10 mm length crystal) and 3 mm for BGO (7 mm length crystal). This depth value is based on the average photon depth of interaction (DOI) for a normally incident 511 keV beam.

To estimate the LSO background of the Inveon system, a 30-minute blank scan was acquired in list-mode format, with an energy window of 350 to 650 keV, yielding approximately 25 counts/s. The blank scan was then combined with simulated data at the list-mode level. For each of the 10 random seeds, a different portion of the blank scan was selected for accurate noise estimation. The same process was used to generate background noise for Genisys4 simulations (approximately 1.8 and 0.24 counts/s for the 150-650 keV and 350-650 keV energy windows, respectively). A time slice-dependent activity issue with GATE was corrected for as described previously.[7]

To estimate position-dependent sensitivity in the Genisys4, we used GATE to simulate a 100 Bq ^{18}F point source enclosed in a 2.5 mm radius sphere of water at static positions within the FOV (3 mm step size in the x, y, and z-coordinates). The sensitivity was then calculated as the fraction of recorded versus expected coincidence events. Since the energy window of the Genisys4 cannot normally be adjusted by the end user from the standard interface, this simulation uses the standard lower level discriminator (LLD) of 150 keV to match the physical phantom experiments.

Trajectory Reconstruction

In summary, the trajectory $\boldsymbol{r}(t)$ of the positron-emitting object is represented as a 3-dimensional B-spline function:

$$\boldsymbol{r}(t) = \sum_{i=1}^{N} \boldsymbol{a}_i B_i(t),$$

where N is the number of spline basis functions, $\boldsymbol{a}_i = (a_i{}^x, a_i{}^y, a_i{}^z)$ are spline coefficients, and $B_i(t)$ are spline basis functions. Details of this method are available in the literature.[7] Reconstruction is performed by solving for the coefficients $\boldsymbol{a}_i$ that minimize the mean-squared distance between the recorded LORs, obtained from list-mode data, and the trajectory estimate. For both the Genisys4 and the Inveon, and under ideal background-free conditions, reconstruction for simulated trajectories was performed using a regularization parameter $\lambda = .005$ and an average of 5 counts per spline interval, as described in Lee et al.[7] This approach simulates the case where velocity of the tracked object is not known a priori. For reconstructions with added background counts, the number of splines was set to match that of the background-free case in each simulation so that differences in trajectories between the 2 cases were not due to the spline representation alone. Furthermore, sampling the source trajectory more finely on the basis of the total number of recorded counts is not justified when the additional background counts contain no useful information. For reconstruction of droplet trajectories from phantom data, the number of counts per spline interval was manually set to a baseline value and adjusted proportionally for each droplet based on velocity and activity. Trajectories were reconstructed and analyzed using MATLAB (Mathworks, Natick, Massachusetts).

Phantom Imaging Experiments With ^{18}F Droplets

A phantom was designed (SolidWorks; Dassault Systèmes, Vélizy-Villacoublay, France) and fabricated by 3D printing a scaffold (Z18; MakerBot Industries, Brooklyn, New York) around which a length of PFA tubing (0.51 mm inner diameter

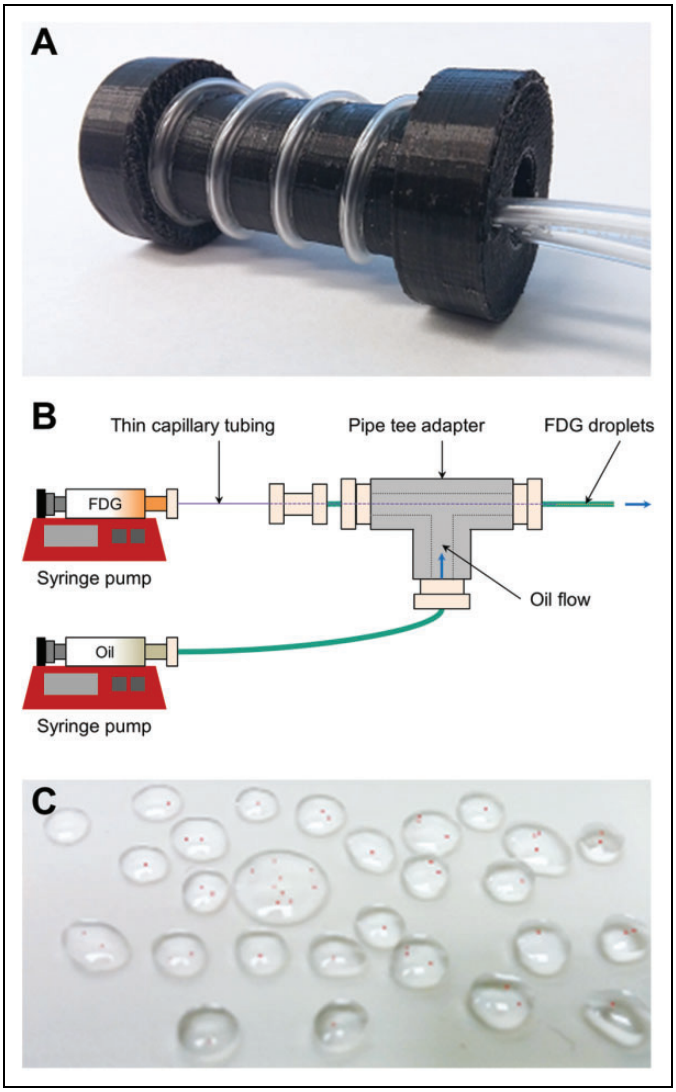

Figure 1. A, Photograph of the phantom. B, Schematics of the droplet generator. C, < 300 μm droplets (red dots) of [18F]fluorodeoxyglucose (FDG) in mineral oil.

[ID], 1.59 mm outer diameter [OD]) was wrapped in a helical fashion (20 mm diameter, 40 mm axial length, 3.89 revolutions), as seen in Figure 1A. The phantom was placed within the FOV of the Genisys4 system. Data were acquired using the default 150 to 650 keV energy window.

Radioactively labeled cells were mimicked with droplets (234-239 μm in diameter) of [^{18}F]FDG (139-296 Bq) in mineral oil using a droplet generator (Figure 1B and C). The droplet generator, based on previous designs,[21,22] consists of a capillary tube with a 50 μm ID and a 360 μm OD inserted into a larger tubing with 500 μm ID. To generate droplets, [^{18}F]FDG mixed with red food coloring (for droplet visualization) was flowed at 0.3 μL/min through the capillary tube and mineral oil at 60 μL/min through the larger tubing in a co-flow configuration. [^{18}F]FDG-filled droplets were then plated onto a glass coverslip and individually selected to be pumped through the phantom using a syringe at rates ranging from 14 to 57 μL/min. List-mode data were acquired for 3 to 5 minutes using the Genysis4 software and imported into MATLAB. After being scanned, droplets were then dropped onto an alcohol wipe and measured 3 consecutive times with a wipe-test counter (Atomlab 500Plus; Biodex Medical Systems, Inc, Shirley, New York).

Computer simulations of the experimental setup were conducted in 2 steps. First, the reconstructed trajectory of the physical droplets was matched by automated rigid registration in MATLAB to the originally planned simulated trajectory (14°/s), generated as described previously. Then, a separate simulation was conducted (using the inverse rigid transformation) to simulate the exact duration, average rotation speed, and average axial translation speed of the droplet's reconstructed trajectory. Simulated activity was estimated from wipe counter readings of the recovered droplet.

Localization Error

The localization error was defined as the mean error of the actual and estimated position throughout the source trajectory in millimeters. For simulated trajectories, where reconstructed and ground truth trajectories were parameterized by time using the same number of points, the average localization error was calculated as:

$$\text{error}_{\text{avg}} = \frac{1}{10}\sum_{s=1}^{10}\left[\frac{1}{5000}\sum_{i=1}^{5000} \| T_s(t_i) - T_0(t_i)\|_2\right]$$

where $s = 1 \cdots 10$ are different statistical simulations of the same experiment, t_i are uniformly spaced time points spanning the entire duration of the experiment, and T_s and T_0 are the reconstructed and ground truth trajectories, respectively. To compare phantom droplet data to matching simulations, the trajectories were reparameterized without a time component due to variability in droplet velocity.

Results

Simulated Sensitivity Profile of the Genisys4

The sensitivity profile of the Genisys4 at the default 150 keV LLD is shown as a cross section in Figure 2. The mean sensitivity throughout the entire FOV was 11.2% ± 3.8% (unless otherwise indicated, means are given hereafter with plus or minus 1 standard deviation). The maximum sensitivity (17.1%) was not achieved at the center of the FOV (14.6%) but rather toward the corner of adjacent panels—this is likely due to a greater number of detector panels potentially involved in the LOR containing these corner positions (3 as opposed to 2 if the source is in the center of the FOV).

Localization Error as a Function of Activity and Rotation Speed

The mean over 10 simulations of the average localization error was calculated for each combination of activity and rotation

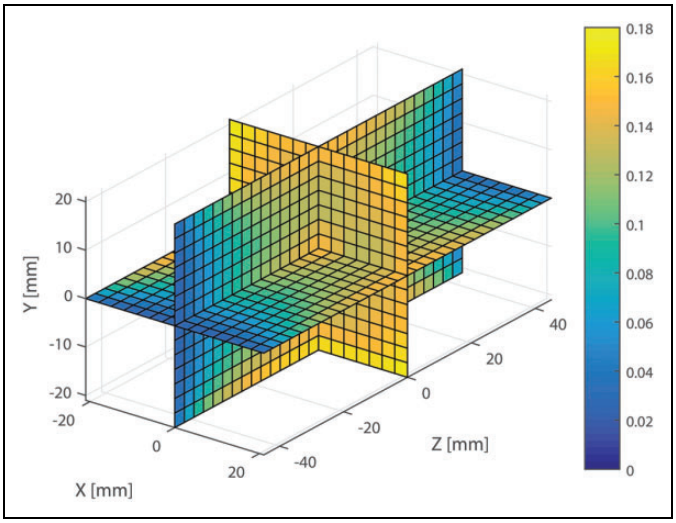

Figure 2. Simulated sensitivity profile of the Genisys4 in three orthogonal planes crossing the origin.

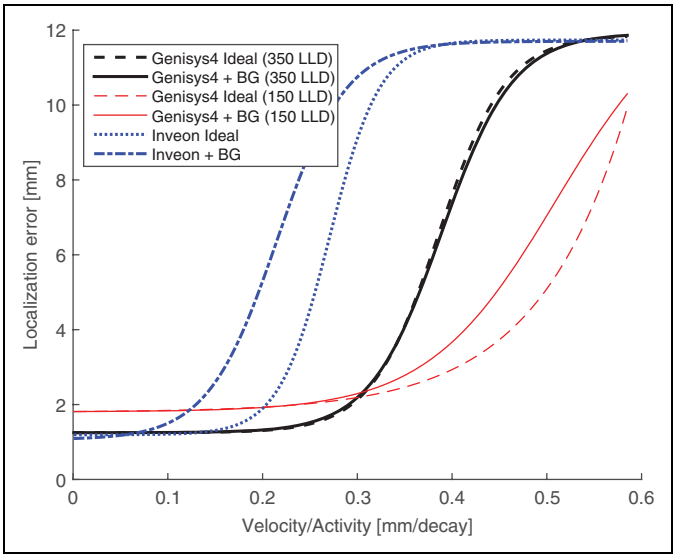

Figure 3. Comparison of simulation performance (average localization error, in mm) as a function of *V*/A, for the Genysis4 and Inveon systems with and without noise and a source activity of 100 Bq or greater.

speed (range of values shown in Table 1). In previous work, we have shown that the localization error is a function of a single parameter, which is the ratio of the source velocity to the source activity (noted as *V*/*A*). The *V*/*A* ratio has units of $\left(\frac{\text{mm}}{\text{s}}\right)/\left(\frac{\text{decay}}{\text{s}}\right) = \text{mm/decay}$ and represents the average distance traveled by the source between 2 decays. However, this role of *V*/*A* only holds in the case of a background-free simulation. When background counts are present, sources with low activity (ie, <100 Bq) will be more difficult to track than those with greater activity, even when the *V*/*A* ratio is the same. To simplify the analysis, we first focus on the case where the activity of the source is greater than 100 Bq. In this case, the localization error can be represented by a function of *V*/*A*. A logistic model of the form:

$$\text{error}_{\text{avg}} = p_1 + \frac{p_2}{1 + \exp\left(-p_3(V/A - p_4)\right)}$$

where p_i are the logistic model parameters, was fit to the average localization errors from the Inveon and Genisys4 systems, both with and without background noise (Figure 3). For all 4 simulation configurations, the goodness of fit (R^2) was greater than 0.99, with the exception of the Inveon with noise for which R^2 was 0.96.

Under the simulated conditions (activity > 100 Bq), localization error of less than 2 mm was achieved at *V*/*A* < 0.29 mm/decay for the Genisys4 with background (350 keV LLD), whereas the Inveon with background required *V*/*A* < 0.13 mm/decay to achieve the same tracking performance. Performance of the 2 systems with noise diverged for *V*/*A* ≥ 0.07 mm/decay. The contribution from LSO background decreased tracking performance of the Inveon under the ideal case by reducing the maximum *V*/*A* for which localization error is less than 2 mm from 0.20 to 0.13 mm/decay. In contrast, the performance of the Genisys4 was not significantly affected by the background when using a 350 keV LLD. The performance of source tracking using a wider 150 keV LLD differs significantly from that achieved with the 350 keV window. The simulations suggest that a wider energy window is detrimental to tracking performance for *V*/*A* < 0.3 mm/decay but advantageous for *V*/*A* > 0.3 mm/decay (Figure 3). This value of *V*/*A* = 0.3 mm/decay likely represents the point beyond which rejecting backscatter with a smaller energy window no longer provides a performance benefit due to the need for counts.

Localization error data from individual systems for simulations with activity ≥100 Bq or <100 Bq can be found in Figure 4. In the latter condition, the ability to track a point source is substantially degraded by background counts, especially for the Inveon system.

Trajectory Reconstruction in a Phantom

Simulation data suggest that the Genisys4 is capable of tracking a moving source within 2 mm when *V*/*A* < 0.29 mm/decay and activity is greater than 100 Bq. To validate this finding, we used the Genysis4 to track the motion of water-in-oil droplets as they moved through a 3D-printed phantom. Figure 5A shows an example of a reconstructed trajectory for a 296-Bq droplet flowed through the phantom at an estimated 3.66 mm/s (*V*/*A* = 0.013 mm/decay; Figure 5B). To further validate the accuracy of the tracking, we compared the measured count rate (over 1 second intervals) along the droplet's trajectory to the predicted sensitivity at the corresponding position in the system's FOV. We found that the 2 quantities were significantly correlated (Pearson correlation $R = .64$, $P << .05$; Figure 5C and D). This demonstrates that the source position estimated using the tracking algorithm is consistent with the sensitivity of the Genisys4 at that position.

On average, the estimated activity of the droplets using the simulated position-dependent sensitivity of the Genysis4 and

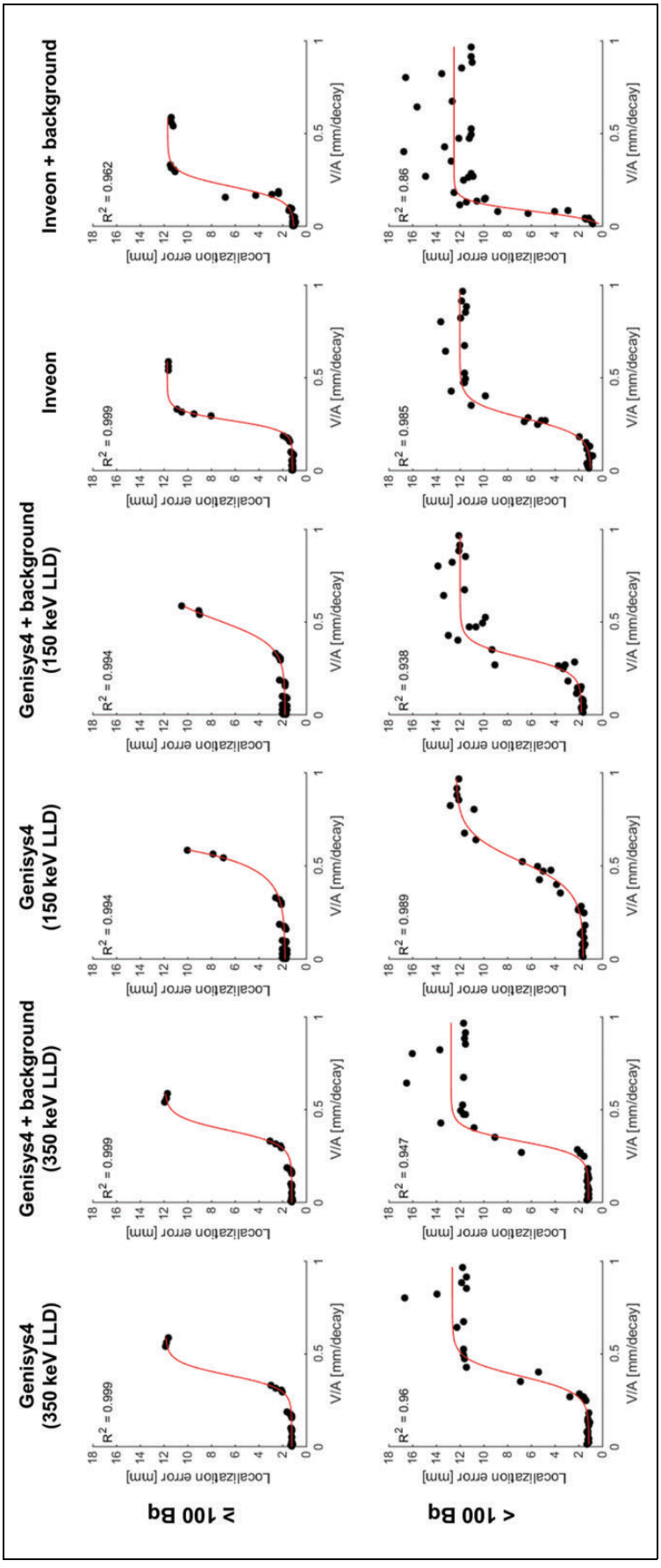

Figure 4. Localization error versus velocity over activity for sources with 100 Bq activity or greater (top row) and sources with less than 100 Bq activity (bottom row).

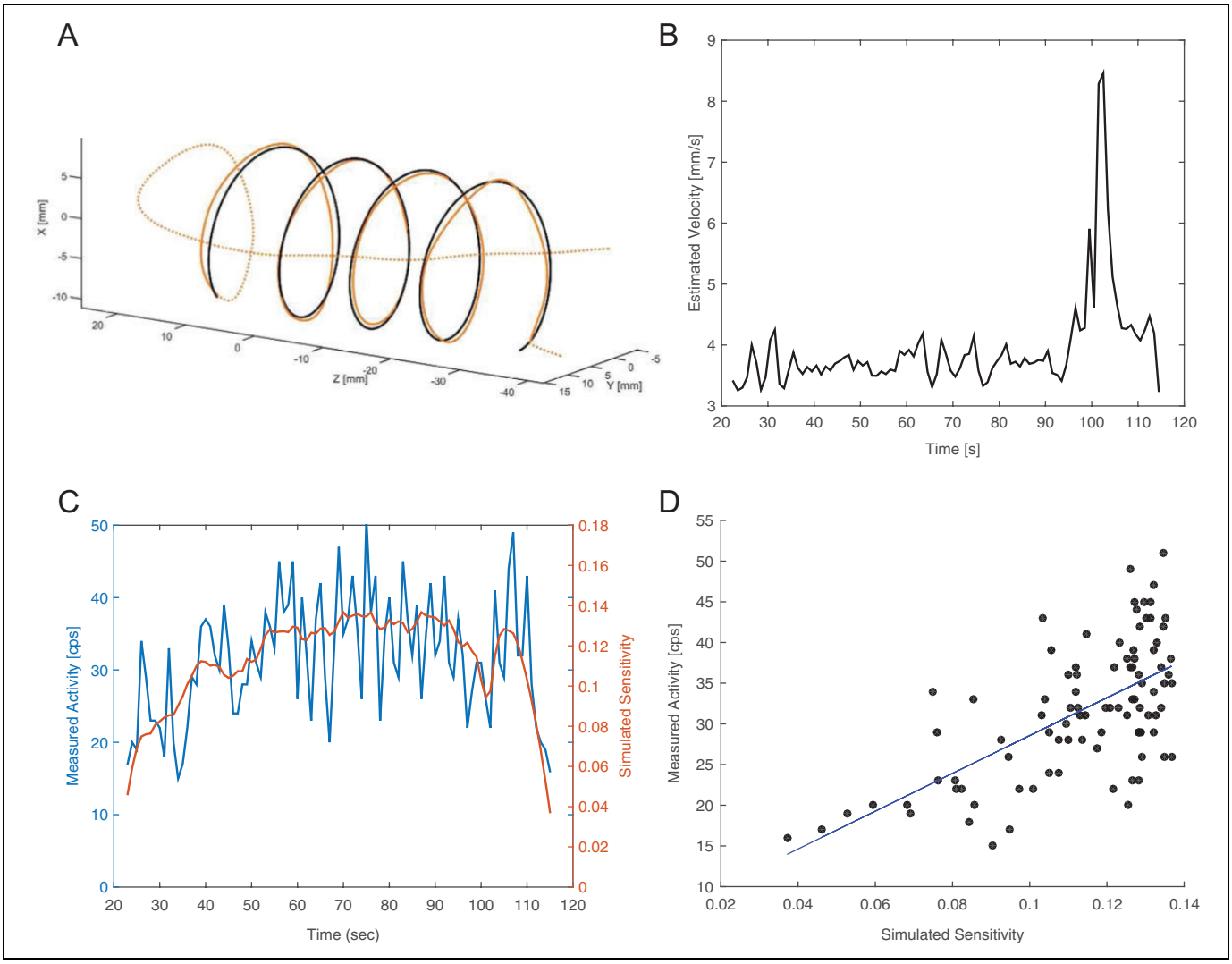

Figure 5. A, Black—simulated ground truth trajectory based on the phantom dimensions and placement within the field of view (FOV). Orange—reconstructed and registered trajectory of a 296 ± 6 (standard error of the mean [SEM]) Bq [18F]-fluorodeoxyglucose (FDG) droplet with an estimated diameter of 240 μm, flowed through the phantom at an estimated 3.8 mm/s. The following subfigures are shown for the entire portion of the trajectory (dotted orange), while localization error was measured based on a subset of the trajectory (solid orange). B, Velocity of the droplet as estimated from the reconstructed trajectory. The increased velocity after 97 seconds corresponds to the droplet passing through a narrowing of the tube as a result of a kink. C and D, Measured counts per second compared to simulated position-dependent sensitivity through the droplet's trajectory shown (C) over time and (D) as a scatterplot (Pearson correlation $R = .64$, $P << .05$).

Table 2. Droplet Reconstruction Results.

Droplet ID	Size, μm[a]	Velocity, mm/s	Activity, Bq[a]	*V*/*A*, mm/decay	Activity Based on List Mode, Bq	Counts per Spline Interval	Simulated Average Localization Error, mm	Average Localization Error, mm
1	235 ± 1	3.77	296 ± 6	0.01	279	40	0.42 ± 0.03	0.62
2	234 ± 4	3.78	160 ± 7	0.02	150	20	0.59 ± 0.03	0.73
3	239 ± 2	1.85	155 ± 4	0.01	143	40	0.41 ± 0.03	0.64
4	234 ± 1	7.33	139 ± 1	0.05	128	10	0.95 ± 0.18	0.83

[a]Given with ± 1 standard error of the mean over 3 measurements

list-mode data was lower than the wipe test counter measurement by 6.9% ± 1.1%. Based on matching simulations, the predicted average localization error of the reconstruction of this droplet was 0.42 ± 0.03 mm. In reality, the measured average localization error of the droplet's trajectory was 0.62 mm, a discrepancy that is likely due to errors introduced by the phantom construction as well as scattering from the phantom materials that were not modeled. Results for other droplets are shown in Table 2.

Discussion

The application of our trajectory reconstruction approach requires an understanding of the characteristics of the system used, as the regime in which the localization error is acceptable will vary depending not only on the object being tracked but also on the geometry and detector characteristics such as noise. In this study, we have examined the position-dependent sensitivity of the Genisys4 system, compared its trajectory reconstruction performance against that of the Inveon, and demonstrated the feasibility of tracking point source-like objects using ^{18}F-FDG droplets. The rationale for this study is that the Genisys4 PET system uses BGO-based detectors, which have no background radioactivity, as opposed to the Inveon PET system that uses LSO crystals in its detectors. Minimizing the background count rate is critical since our goal is to track very weak sources.

GATE simulations suggest that the Genisys4 is capable of tracking ^{18}F sources with less than 2 mm localization error for V/A up to 0.29 mm/decay (Figure 3). For a source activity of 100 Bq, this amounts to a velocity of up to 29 mm/s. The Inveon exhibits poorer performance, even under an ideal case without LSO background (Figure 3), which suggests the important role that system sensitivity plays with respect to trajectory reconstruction performance. Our phantom experiments showed that tracking ^{18}F sources with greater than 100 Bq at $V/A < 0.05$ mm/decay is feasible with localization error less than 1 mm (Figure 4 and Table 2).

A priori knowledge of the approximate velocity of the tracked object, particularly the upper bound, is expected to reduce localization error. For example, in our simulations, the naive approach of fixing the number of counts per spline interval at 5 resulted in underestimating the system's performance, particularly at higher counts. Results from our phantom and matched simulation data show that less than 1 mm localization error is achievable. For a 1000 Bq source moving helically with 4°/s rotation, localization error is improved from 1.16 ± 0.02 mm to 0.30 ± 0.02 mm by increasing the number of counts per spline interval from 5 to 50 (see Supplemental Figure 1). By increasing the counts per spline interval another 10-fold to 500, localization error is further reduced to 0.10 ± 0.01. However, prior knowledge of a tracked object's velocity may not always be known and/or constant. A possible approach is adjusting counts per spline interval a posteriori as an optimization parameter.

Performance would further benefit from increased signal-to-noise in the acquired list-mode data. Improved results may have been achieved with better centering of the phantom due to position-dependent sensitivity, particularly along the axial direction. In addition, while the default energy window of 150 to 650 keV is not easily adjustable by the end user, we expect a reduced energy window of 350 to 650 keV to improve tracking performance under certain conditions ($V/A < 0.30$ mm/decay) due to a lower background count rate from fewer accepted backscatter events.[18] The assignment of LORs based on more accurate DOI estimation methods may also improve reconstruction results, particularly for trajectories that are off-center.

In conclusion, in this work, we have investigated the feasibility of tracking the movement of small point-source-like positron-emitting objects using a trajectory reconstruction technique with list-mode data acquired by the Genisys4 PET system. In silico simulations suggest that tracking performance is significantly better for this system than for the Inveon due to LSO background. These results, in addition to preliminary data acquired using a moving ^{18}F droplet phantom, suggest the merit of using BGO-based PET systems for trajectory reconstruction applications. Further work, including optimization of cell radiolabeling and independent confirmation of such results, will be necessary to apply the Genisys4 PET system to tracking live radiolabeled cells in vivo.

Acknowledgments

We would like to thank Hongquan Li and Frezghi Habte for help with the Genisys4 system.

Declaration of Conflicting Interests

The author(s) declared no potential conflicts of interest with respect to the research, authorship, and/or publication of this article.

Funding

The author(s) disclosed receipt of the following financial support for the research, authorship, and/or publication of this article: This work was supported by a postdoctoral training fellowship from the National Institute of Health (5T32CA121940), and a grant from the NIH National Heart, Lung, and Blood Institute (R21HL127900).

Supplemental Material

The online Supplemental Figure is available at http://mix.sagepub.com/supplemental.

References

1. Kircher MF, Gambhir SS, Grimm J. Noninvasive cell-tracking methods. *Nat Rev Clin Oncol*. 2011;8(11):677-688.
2. Yu M, Stott S, Toner M, Maheswaran S, Haber DA. Circulating tumor cells: approaches to isolation and characterization. *J Cell Biol*. 2011;192(3):373-382.
3. Krebs MG, Hou JM, Sloane R, et al. Analysis of circulating tumor cells in patients with non-small cell lung cancer using epithelial marker-dependent and-independent approaches. *J Thorac Oncol*. 2012;7(2):306-315.
4. Wang X, Qian X, Beitler JJ, et al. Detection of circulating tumor cells in human peripheral blood using surface-enhanced Raman scattering nanoparticles. *Cancer Res*. 2011;71(5):1526-1532.
5. Zhang Y, Dasilva JN, Hadizad T, et al. 18F-FDG cell labeling may underestimate transplanted cell homing: more accurate, efficient, and stable cell labeling with hexadecyl-4-[18F] fluorobenzoate for in vivo tracking of transplanted human progenitor cells by positron emission tomography. *Cell Transplant*. 2012; 21(9):1821-1835.

6. Ma B, Hankenson KD, Dennis JE, Caplan AI, Goldstein SA, Kilbourn MR. A simple method for stem cell labeling with fluorine 18. *Nucl Med Biol*. 2005;32(7):701-705.
7. Lee KS, Kim TJ, Pratx G. Single-cell tracking with PET using a novel trajectory reconstruction algorithm. *IEEE Trans Med Imaging*. 2015;34(4):994-1003.
8. Shapiro EM, Sharer K, Skrtic S, Koretsky AP. In vivo detection of single cells by MRI. *Magn Reson Med*. 2006;55(2):242-249.
9. Heyn C, Ronald JA, Mackenzie LT, et al. In vivo magnetic resonance imaging of single cells in mouse brain with optical validation. *Magn Reson Med*. 2006;55(1):23-29.
10. Rogers WJ, Meyer CH, Kramer CM. Technology insight: in vivo cell tracking by use of MRI. *Nat Clin Pract Cardiovasc Med*. 2006;3(10):554-562.
11. Zhang Z, van den Bos EJ, Wielopolski PA, et al. In vitro imaging of single living human umbilical vein endothelial cells with a clinical 3.0-T MRI scanner. *MAGMA*. 2005;18(4):175-185.
12. Heyn C, Bowen CV, Rutt BK, Foster PJ. Detection threshold of single SPIO-labeled cells with FIESTA. *Magn Reson Med*. 2005; 53(2):312-320.
13. Bemrose CR, Fowles P, Hawkesworth MR, O'Dwyer MA. Application of positron emission tomography to particulate flow measurement in chemical engineering processes. *Nucl Instrum Meth A*. 1988;273(2):874-880.
14. Pérez-Mohedano R, Letzelterb N, Amadorb CT, Bakalisa VS. Positron emission particle tracking studies of spherical particle motion in rotating drums. *Chem Eng Sci*. 1997;52(13): 2011-2022.
15. Bao Q, Chatziioannou AF. Estimation of the minimum detectable activity of preclinical PET imaging systems with an analytical method. *Med Phys*. 2010;37(11):6070-6083.
16. Bai B, Dahlbom M, Park R, et al. Performance comparison of GENISYS4 and microPET preclinical PET scanners. In: *IEEE Nuclear Science Symposium and Medical Imaging Conference (NSS/MIC)*, Anaheim, CA, USA, 27 October-3 November 2012, pp. 3765-3768. New York: IEEE.
17. Lewis TA. The reduction of background signal in bismuth germanate scintillators. *Nucl Instrum Meth A*. 1988;264(2): 534-535.
18. Gu Z, Bao Q, Taschereau R, Wang H, Bai B, Chatziioannou AF. Optimization of the energy window for PETbox4, a preclinical PET tomograph with a small inner diameter. *IEEE Trans Nucl Sci*. 2014;61(3):1164-1173.
19. Gu Z, Taschereau R, Vu NT, et al. Design and initial performance of PETbox4, a high sensitivity preclinical imaging tomograph. In: *IEEE Nuclear Science Symposium and Medical Imaging Conference (NSS/MIC)*, Valencia, Spain, 23 October-29 October 2011, pp. 2328-2331. New York: IEEE.
20. Gu Z, Taschereau R, Vu NT, et al. NEMA NU-4 performance evaluation of PETbox4, a high sensitivity dedicated PET preclinical tomograph. *Phys Med Biol*. 2013;58(11):3791-3814.
21. Terray A, Hart SJ. "Off-the-shelf" 3-D microfluidic nozzle. *Lab Chip*. 2010;10(13):1729-1731.
22. Wu P, Wang Y, Luo Z, Li Y, Li M, He L. A 3D easily-assembled Micro-Cross for droplet generation. *Lab Chip*. 2014;14(4): 795-798.